
Article:
Tang, Zhichuan, Yang, Keshuai, Wang, Hang et al. (4 more authors) (2024) Bio-inspired soft pneumatic actuator based on a Kresling-like pattern with a rigid skeleton. Journal of Advanced Research. pp. 91-102. ISSN 2090-1232

https://doi.org/10.1016/j.jare.2023.10.004

Journal of Advanced Research 63 (2024) 91–102

Contents lists available at ScienceDirect

Journal of Advanced Research

journal homepage: www.elsevier.com/locate/jare

Bio-inspired soft pneumatic actuator based on a kresling-like pattern with a rigid skeleton

Zhichuan Tang [a,b,*], Keshuai Yang [a], Hang Wang [a], Zhixuan Cui [a], Xiaoneng Jin [a], Yuxin Peng [c], Pengcheng Liu [d]

[a] Industrial Design Institute, Zhejiang University of Technology, Hangzhou 310014, China
[b] Modern Industrial Design Institute, Zhejiang University, Hangzhou 310013, China
[c] College of Education, Zhejiang University, Hangzhou 310058, China
[d] Department of Computer Science, University of York, York YO10 5DD, United Kingdom

HIGHLIGHTS

- We proposed an SPA based on a Kresling-like pattern with a rigid skeleton by observing the cloning and moving behaviors from salps.
- An extensible inserting structure is innovatively designed to replace the creases in traditional Kresling patterns.
- The SPA can perform an axial contraction motion without twisting and a controllable bending motion.
- The number of layers of Kresling-like patterns is changeable by adding or reducing skeleton components.
- The elongation can reach to above 162% and the output force can reach to above 6.36 N.

GRAPHICAL ABSTRACT

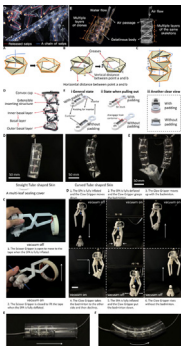

ARTICLE INFO

Article history:
Received 15 June 2023
Revised 28 September 2023
Accepted 4 October 2023
Available online 12 October 2023

Keywords:
Bio-inspired
Soft actuator
Kresling-like pattern
Salps
Rigid skeleton

ABSTRACT

Introduction: Biomimetic soft pneumatic actuators (SPA) with Kresling origami patterns have unique advantages over conventional rigid robots, owing to their adaptability and safety.
Objectives: Inspired by cloning and moving behaviors observed from salps, we proposed an SPA based on a Kresling-like pattern with a rigid skeleton. The elongation and output force were tested, and the effectiveness of the applications with the SPA was evaluated.
Methods: The proposed SPA consists of rigid skeletons and a soft skin. The rigid skeletons are constructed using layers of Kresling-like patterns, while a novel extensible inserting structure is devised to replace the folds found in conventional Kresling patterns. This innovative approach ensures that the SPA exhibits axial contraction/expansion motion without any twisting movement. To mimic the bionic characteristics of swimming and ingesting progress of salps, the proposed SPA can perform an axial contraction motion without twisting and a controllable bending motion based on multi-layered Kresling-like patterns; to mimic the cloning and releasing life phenomena of salps, the number of layers of Kresling-like patterns is changeable by adding or reducing skeleton components according to the practical needs.
Results: The experimental elongation results on the SPA with multiple layers of Kresling-like patterns show that the elongation can increase to above 162% by adding layers; the experimental output force results show that the three-layer SPA can provide 6.36 N output force at an air flow rate of 10 L/min,

* Corresponding author at: Industrial Design Institute, Zhejiang University of Technology, Hangzhou 310014, China.
E-mail address: ztang@zjut.edu.cn (Z. Tang).

https://doi.org/10.1016/j.jare.2023.10.004

and the output force will continue to increase as the number of layers of Kresling-like pattern increases or the air flow rate increases. Further, we demonstrate the applications of the SPA in soft grippers, scissor grippers, claw grippers and pipe crawlers.
Conclusion: Our proposed SPA can avoid twisting in the radial contraction motion with high elongation and output force, and provide the practical guidance for bio-inspired soft robotic applications.

Introduction

Soft actuators are core components to develop the soft robotics due to their adaptability and safety [1–3], and they have been widely used in medical [4–6], biological [7–9], and rehabilitation fields [10–13]. The actuation methods of soft actuators include variable-length tendon, fluidic/pneumatic actuation, and intelligent materials with electrical, thermal and magnetic stimuli [7,14–18]. Among them, the pneumatic actuation is reported frequently to be applied in the soft actuators, which achieve axial contraction/expansion motion, rotation, bending, and twisting in different practical applications [19]. The soft pneumatic actuators (SPAs) can be controlled by air flow to realize continuous deformation as a quick response to air pressure stimulus, resulting in better human–machine interaction and operation experiences in the complex working environments [20,21].

As one of compliant mechanisms, foldable origami has been widely applied in the design of the SPAs, as it allows reshaping of planar materials into three-dimensional (3D) architectures for realizing specific robotic motion patterns [22]. Kresling origami pattern inspired by the leaf model [23] has been as a basic unit structure in some origami-based SPAs with the capability of multimodal deformation, and it brings certain desirable characteristics for different applications, such as controllable contraction/expansion motion and continuous bending motion according to modify its construction [22,24,25]. Some previous studies fabricated a series of actuators based on the Kresling origami structure. Ze et al. applied Kresling units to propose an magnet-actuated origami crawler which could perform contraction and expansion motions, and the crawler was safely used for the drug storage and release in human body because of the small scale and the flexible material [4]; Zhang et al. proposed a novel pneumatic/cable-driven hybrid linear actuator with Kresling origami chambers, and the actuator could perform linear bidirectional motions but could not perform bending motion [26]; Jin et al. developed a low-cost vacuum-powered SPA consisted of multiple cubes with Kresling patterns, and the SPA could achieve worm-like creep, bending motion and obstacle detection [27]. These SPAs with Kresling patterns in above studies have many features like lightweight, compliance and safety [28,29]. However, it should be noted that traditional SPAs employing Kresling patterns are prone to experiencing twisting motion during axial contraction/expansion movements [30], which is not applicable to some usage scenarios where we only need the axial contraction/expansion motion (e.g., gripper application and bending application) and causes energy loss unnecessarily [31]. In addition, the fabrication process of some traditional SPAs is complex and takes a long time [32,33], and most of them are difficult to add/reduce layers of Kresling patterns or disassemble/assemble the skeleton components repeatedly according to the practical needs [34].

By observing the moving and morphing behaviors of soft-bodied creatures, several motion modes can be discovered [35–37]. Inspired by the octopus arms' features such as large and continuous deformations, adjustable compliance, and agile motions for moving and preying. Wu et al. explored the compliant mechanisms like foldable origami, which allow reshaping of planar materials or structures into intricate three-dimensional architectures in various scales for robotic motions [22]; Rayner et al. developed the recyclable, reconfigurable and recoverable VAMPs with mechanical design that can allow the basic system to operate as a joint, a muscle or a bone by combining vacuum operation and variable sleeve properties to actuate or jam the actuators just like creatures' bodies [38]; Inspired by the pelican eel's stretchable and foldable frames, Kim et al. developed dual-morphing SPA architectures that embody quasi-sequential behaviors of origami unfolding and skin stretching in response to fluid pressure [39]. These biological moving/morphing behaviors have been as a central design strategy of SPAs in many cases. However, few studies have focused on the biological life behaviors in SPAs to meet the potential design demands for modularization and customization. Based on demands of modularization and customization, SPAs are supposed to be formed with similar units that can be repeatedly disassembled or assembled. Furthermore, the number of units in one SPA are supposed to be determined by our demands for the scale of the SPA. We found that salps can reproduce child organisms through asexual cloning, and each clone of salps can separate from parent blastozooids freely. These life behaviors perfectly match our requirements for modularization. According to our investigation, a salp is a barrel-shaped planktonic tunicate (Fig. 1A) [40] that pumps water across a mucous mesh using muscular pumping that also propels the animal through the water (Fig. 1B) [41]. The complex life history of salps comprises an alternation of generations between asexual solitary animals and sexually reproducing clonal chains (Fig. 1C) [42]. With the observation on salps, we found that the biological life behaviors of salps provides valuable guidance for modular design of the SPA. Our SPA was therefore designed by mimicking the behavior of salps in nature: (1) Many aggregate salps (known as blastozooids) form a chain when they are moving and feeding and grow together, which inspired us to connect all SPA's units together and design one shared air passage for these units. (2) One individual in the chain of salps can be regarded as a "layer", which inspired us to design the multiple-layer structure that can add or remove layers based on the practical needs to achieve axial contraction/expansion and bending motions.

In our paper, inspired by both cloning behaviors and moving behaviors observed from salps (Fig. 1E), we developed a soft pneumatic actuator (SPA) based on a Kresling-like pattern with a rigid skeleton. To mimic the bionic characteristics of swimming and ingesting progress of salps, the proposed SPA can perform an axial contraction motion without twisting and a controllable bending motion based on multi-layered Kresling-like patterns; to mimic the life phenomena of a salp cloning itself and releasing from parent blastozooids, the number of layers of Kresling-like patterns is changeable by adding or reducing skeleton components according to the practical needs, i.e., modular design. The proposed SPA consists of rigid skeletons and a soft skin. The rigid skeletons are built by Kresling-like pattern layers, i.e., basic Kresling-like units. We innovatively designed an extensible inserting structure to replace the creases in traditional Kresling patterns, resulting in no twisting motion when the SPA with Kresling-like patterns performs the axial contraction/expansion motion. We can easily fabricate rigid skeletons by 3D printing [43], and disassemble or assemble the

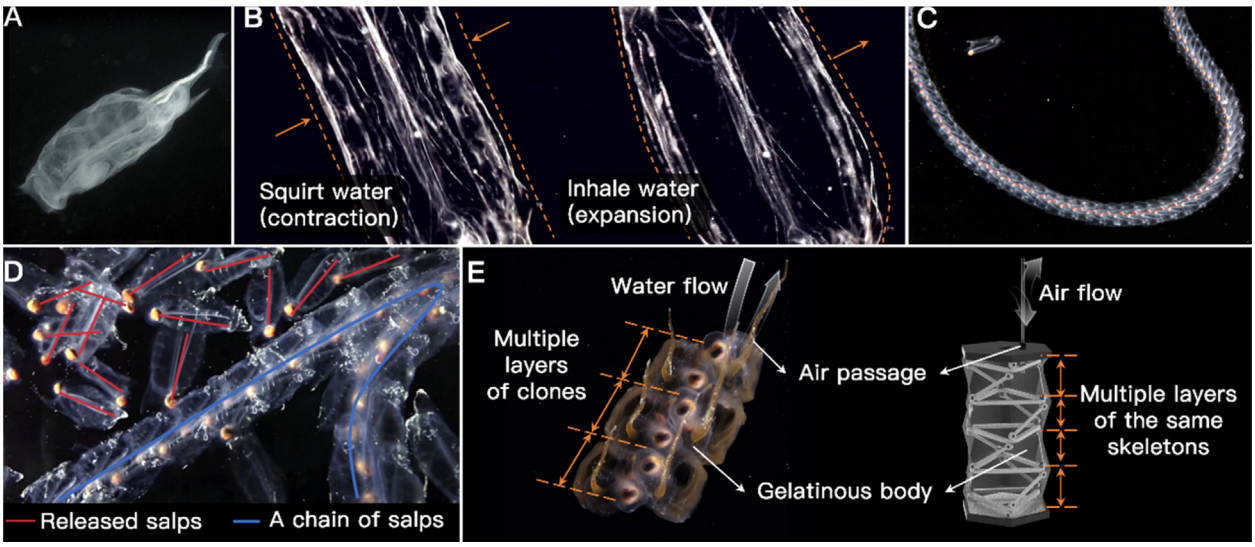

Fig. 1. Biological characteristics observed from salps. (A) One salp in the ocean. (B) Two states of salps when they are moving by pumping water: contraction after squirting water (left) and expansion after inhaling water (right). (C) A chain of slaps formed by a number of individuals. (D) The growing salps are released from the chain. The pink lines represent the released salps, and the blue line represents a chain of salps. (E) Inspired by the cloning, releasing, moving, and feeding patterns of salps, the prototype of the SPA based on Kresling-like patterns with a rigid skeleton is built. The SPA has a shared air passage, a soft skin, and multi-layer skeletons, which are corresponding to salps' shared air passage, gelatinous body, and clones, respectively. (For interpretation of the references to colour in this figure legend, the reader is referred to the web version of this article.)

basic Kresling-like units repeatedly. The soft skin that mimics the salp's gelatinous body is sealed by a heat sealer and fixed by sandwich sealing structures. The multi-shape skins are produced by different sealing methods to realize different motions. To learn from the nature of growing together when salps are swimming and feeding, the air passage throughout the entire SPA is designed to ensure that the axial contraction/expansion and bending motions happen in all layers together.

Material and methods

The structure design of a basic kresling-like unit

As shown in Fig. 2A, a traditional Kresling pattern couples axial contraction motion with twisting motion under external forces [4,44]. In order to capture the essential behaviors of the Kresling pattern, we model Kresling pattern as a truss structure as shown in Fig. 2B, and assume that all the out-of-axis deformations of the top and bottom surfaces are small enough to be ignored. We also assume that the bottom surface is fixed. The top and bottom surface of the truss are modeled as rigid frames while creases are modeled to be deformable [45,46]. The proposed model explains the coupled twist. For example, the horizontal distance between point *a* and point *b* increases with the decreasing vertical distance between point *a* and point *b*, and then the point *b* will move closer to the *de*-axis symmetrical point *c*. All creases in the Kresling pattern will move like *ab*, resulting in a twisting motion. To eliminate the twisting motion, the traditional method is adding another Kresling pattern unit with the reverse creases [46], as shown in Fig. 2C. However, this method must ensure that the number of Kresling units is even, and it still cannot eliminate the twisting motion for each individual unit [47]. Thus, the number of layers is limited if we don't need the twisting motion when the SPA with traditional Kresling pattern performs the traditional Kresling pattern.

The solution of this paper is to design an extensible inserting structure by 3D printing to replace the creases in traditional Kresling patterns. The reason of the coupled twisting motion is that the length of each crease is unchangeable, so we let the new "crease" (i.e., extensible inserting structure) be adjustable. This Kresling-like structure eliminates the coupled twisting motion, and retains the features of the Kresling origami. Another advantage of this solution is that the extensible inserting structure can be disassembled or assembled easily and repeatedly to form the skeleton with different layers, which results in a simplified fabrication process.

Fig. 2D shows a four-layer skeleton of our proposed SPA with extensible inserting structures. The top and bottom parts of each layer (i.e., a basic Kresling-like unit) are called "basal plate", which is further classified into "inner basal plate" and "outer basal plate" according to the different location. Every two adjacent layers share one "inner basal plate". The "basal plate" and extensible inserting structures are connected by the "convex cap". Each basic Kresling-like unit includes three extensible inserting structures (Fig. 2E) which consist of three components: "inserter", "padding for inserter", and "container". The "inserter" with a bump is inserted into the "container", and the "padding for inserter" is used to elevate the position of the "inserter". When we pull out the "inserter" and "padding for inserter" together, it will be stuck and not separate from the "container" due to the bump. Fig. 2E also shows the extensible inserting structure with and without padding under general state and pulling state.

Fabrication of the SPA

As shown in Fig. 3A, the SPA we designed consists of a rigid skeleton with Kresling-like patterns, a soft skin, and two sandwich sealing structures.

The rigid skeleton consists of extensible inserting structures, basal plates, and convex caps. The extensible inserting structure is made of high-toughness resin (Wenext 8500), and it consists of an inserter, a padding for inserter, and a container (Fig. 3B). The height of the inner hollow space of the container (W_{Con}) is 2 mm; the height of the thickest part of the inserter ($W_{Ins\text{-}Max}$) is 1.5 mm, and the height of the thinnest part of the inserter ($W_{Ins\text{-}Min}$) is 0.5 mm; the height of the padding for inserter (W_{Pad}) is 1 mm. The steps of the installation process are as follows: (1) insert the inserter into the container ($W_{Con} > W_{Ins\text{-}Max}$); (2) insert the pad-

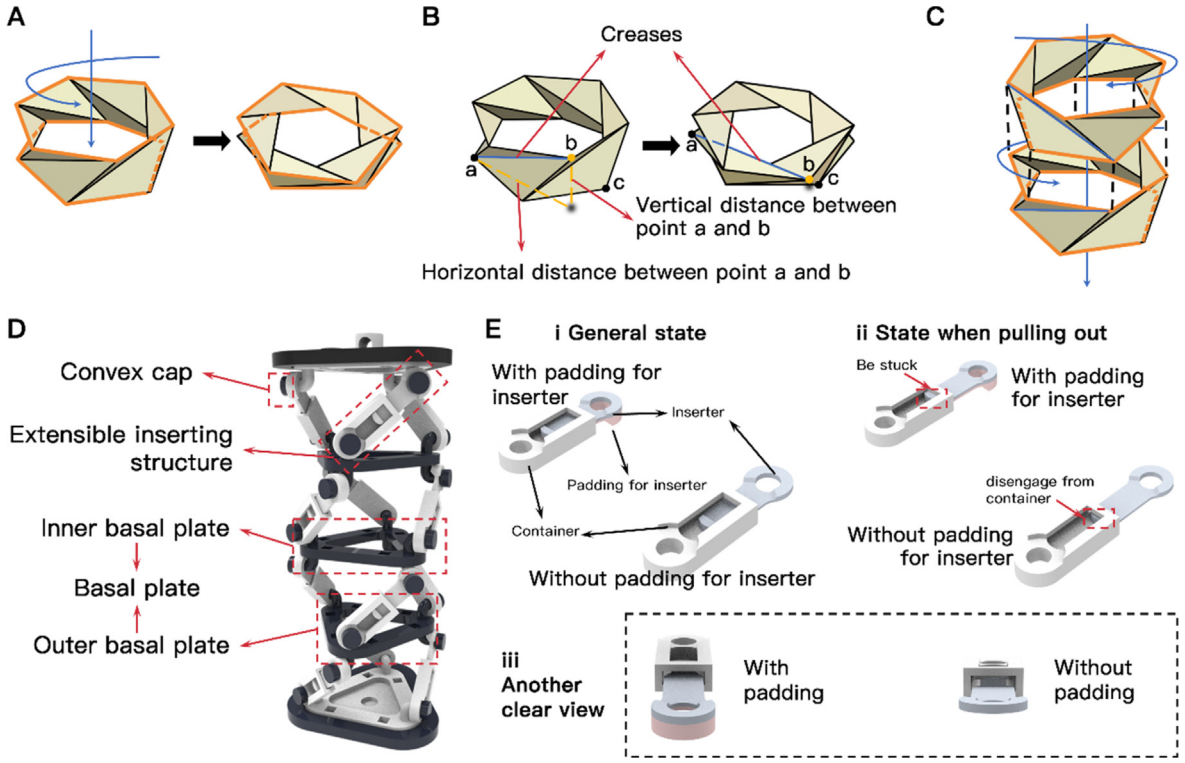

Fig. 2. The design of a unit of Kresling-like patterns and the evolution from creases to extensible inserting structures. (A) A traditional Kresling pattern couples axial contraction motion with twisting motion under external forces. The highlighted lines represent the top and bottom sides in one Kresling unit. The top side happens the twisting motion when we press the unit. (B) The graphic expression of the coupled twisting motion. The reason of the coupled twisting motion is that the length of creases (blue lines) of each Kresling pattern unit is unchangeable when the unit performs the axial contraction motion. For example, the horizontal distance between point *a* and point *b* increases with the decreasing vertical distance between point *a* and point *b*, and then the point *b* will move closer to the *de*-axis symmetrical point *c*. All creases in the Kresling pattern will move like *ab*, resulting in a twisting motion. (C) An existing method to eliminate the coupled twisting motion. Another Kresling pattern unit with the reverse creases is added to perform the twisting motion in opposite direction, and the twisting motions of two units will cancel each other out. (D) The top and bottom parts of each layer (i.e., a basic Kresling-like unit) are called "basal plate", which is further classified into "inner basal plate" and "outer basal plate" according to the different locations. Every two adjacent layers share one "inner basal plate". The "basal plate" and extensible inserting structures are connected by the "convex cap". (E) The components of the extensible inserting structure. The grey component is the "inserter", the pink component is the "padding for inserter", and the white component is the "container". The "inserter" with a bump is inserted into the "container", and the "padding for inserter" is used to elevate the position of the "inserter". When we pull out the "inserter" and "padding for inserter" together, they will be stuck and not separate from the "container" due to the bump at the end of the "inserter". The extensible inserting structure with and without padding under general state and pulling state are shown in this figure. (For interpretation of the references to colour in this figure legend, the reader is referred to the web version of this article.)

ding for inserter into the container and place it beneath the inserter ($W_{Con} > W_{Ins\text{-}Min} + W_{Pad}$). After the extensible inserting structure is attached onto the basal plate, the inserter will not separate from the container when the extensible inserting structure moves ($W_{Con} < W_{Ins\text{-}Max} + W_{pad}$). The L-shaped parts with convex caps are used to connect the extensible inserting structures and the basal plates (Fig. 3C). There are cuboids on the ends of the L-shaped parts, and the length of the cuboid is slightly larger than the diameter of the end of the L-shaped part. The convex cap with a hollow space that matches the structure of the end of the L-shaped part is used to fix the extensible inserting structure. The diameter of the hollow space is slightly larger than the diameter of the end of the L-shaped part. The steps of the installation process are as follows: (1) put the convex cap on the end of the L-shaped part when the cuboid on the end of the L-shaped part is inserted into the hollow space of the convex cap; (2) rotate the convex cap clockwise about 1/4 turn; (3) press the convex cap and lock it on the end of the L-shaped part. Basal plates in one SPA include inner basal plates and outer basal plates according to the different positions, as shown in Fig. 3D. Compared to the inner basal plate, the outer basal plate only has three L-shaped parts and include an additional cylinder component (the diameter is 8 mm, and the height is 6.7 mm) on the top surface. A hole (the diameter is 4.2 mm) in the cylinder component is used to connect the SPA and the aluminum framework. The outer basal plate which is used to connect the air tube has an additional hole (diameter is 4.5 mm) as the air flow inlet.

According to the motion and biomimetic requirement of the SPA, the high-toughness polyethylene (PE), which possesses a transparent skin just as a salp's gelatinous body does, is selected as the material of the soft skin. The PE material is further processed by folding and heat sealing to form the different shapes of the soft skins, corresponding to the deformations of salp chains. As shown in Fig. 3E, for the SPA to perform the axial contraction/expansion motion, the PE materials are folded in half and heat-sealed to form a straight tube-shaped skin; for the SPA to perform the bending motion, the PE materials are folded several times in a zig-zag pattern until the length of the folded skin is same as the expected length of the short side of the bending SPA, and then is heat-sealed to form a curved tube-shaped skin. After putting the rigid skeleton inside of the soft skin, the two ends of the soft skin are fixed and clamped by the sandwich sealing structures.

As shown in Fig. 3F, a sandwich sealing structure consists of three components: an outer basal plate, a sealing cover, and a sealing bolt. The outer basal plate and the sealing cover are used to clamp the two ends of the soft skin, and the sealing bolt is used to fix this structure. There is a hollow space corresponding to the shape of the outer basal plate on the bottom surface of the sealing

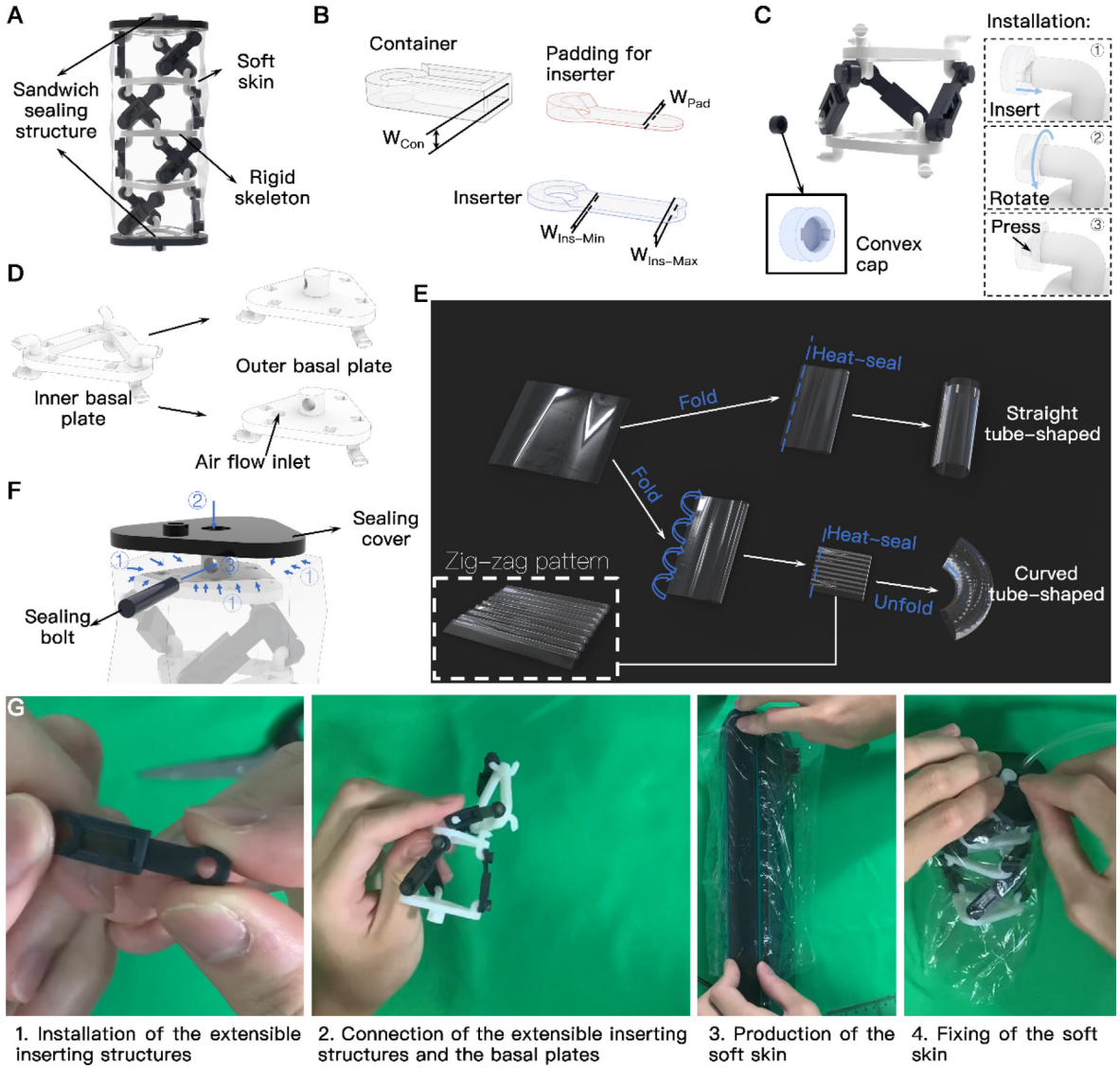

Fig. 3. Fabrication of the SPA. (A) The whole structure of the SPA. The SPA consists of a rigid skeleton with Kresling-like patterns, a soft skin, and two sandwich sealing structures. Two ends of the SPA are clamped by the sandwich sealing structures. The rigid skeleton is wrapped in the soft skin. (B) The schematic diagram of three components (an inserter, a padding for inserter, and a container) in an extensible inserting structure. The height of the inner hollow space of the container (W_{Con}) is 2 mm; the height of the thickest part of the inserter ($W_{Ins\text{-}Max}$) is 1.5 mm, and the height of the thinnest part of the inserter ($W_{Ins\text{-}Min}$) is 0.5 mm; the height of the padding for inserter (W_{Pad}) is 0.5 mm. (C) The steps of the installation process for the convex cap. The L-shaped parts with convex caps are used to connect the extensible inserting structures and the basal plates. The convex cap with a hollow space that matches the structure of the end of the L-shaped part is used to fix the extensible inserting structure. The steps of the installation process are as follows: (1) put the convex cap on the end of the L-shaped part when the cuboid on the end of the L-shaped part is inserted into the hollow space of the convex cap; (2) rotate the convex cap clockwise about 1/4 turn; (3) press the convex cap and lock it on the end of the L-shaped part. (D) The schematic diagram of different basal plates. Basal plates in one SPA include inner basal plates and outer basal plates according to the different positions. Compared to the inner basal plate, the outer basal plate only has three L-shaped parts and include an additional cylinder component on the top surface. The outer basal plate which is used to connect the air tube has an additional hole as the air flow inlet. (E) The folding and heat-sealing process of the different shapes of the soft skins for the different SPAs to perform the axial contraction/expansion motion and bending motion. (F) The schematic diagram of a sandwich sealing structure. The sandwich sealing structure consists of three components: an outer basal plate, a sealing cover, and a sealing bolt. The outer basal plate and the sealing cover are used to clamp the two ends of the soft skin, and the sealing bolt is used to fix this structure. The steps to fix the soft skin by the sandwich sealing structure are as follows: (1) fold the ends of the soft skin inward; (2) the soft skin is sandwiched between the sealing cover and the outer basal plate; (3) insert the sealing bolt to prevent the separation between the sealing cover and the outer basal plate. (G) Installation of the SPA includes: (1) install the extensible inserting structure; (2) connect the extensible inserting structures and the basal plates; (3) fold and seal the soft skin; (4) fix the soft skin.

cover. A hole at the center of the sealing cover is for the entrance of the cylinder component on the outer basal plate; a hole on the sealing cover corresponding to the hole on the outer basal plate is used to connect the air tube. The sealing bolt is a cylinder with a diameter of 4 mm and a length of 22 mm, which is inserted into the hole of the cylinder component on the outer basal plate. The progression of fixing the soft skin by the sandwich sealing structure include two steps. Firstly, the ends of the soft skin are folded inward between the sealing cover and the outer basal plate; then, the sealing bolt is inserted to prevent the separation between the sealing cover and the outer basal plate.

Installation of the SPA

When the SPA is installed, we firstly install the extensible inserting structures, i.e., insert the inserter into the container, and then insert the padding for inserter into the container and place it beneath the inserter. Secondly, we connect the the extensible inserting structures to the L-shaped parts, and use the convex caps to lock them. Thirdly, we fold and seal the PE materials to form the soft skin according to different shapes and requirements. Lastly, we put the rigid skeleton into the soft skin, fix it with sandwich sealing structures. Fig. 3G illustrates the installation process

above in detail. Movie S1 shows the installation process of an SPA with three-layer Kresling-like patterns, and its contraction/expansion motion performance is tested. The installed SPA can perform the contraction motion and the expansion motion smoothly controlled by the negative/positive pressure. The installation method allows us to adjust the structure of the SPA easily, such as adding or removing layers, changing the material of the soft skin, etc.

The elongation

As the skeleton in the Kresling-like unit is physically rigid, it is expected that varying the geometric parameters of the skeleton (e.g., the scale of 3D printing components) can provide a means to adjust the elongation (e) of the Kresling-like unit. To interrogate the underlying mathematical relationship between the elongation and geometric parameters of the skeleton, we used SOLIDWORKS to model all components and simulate the contraction motion. We defined the parameters in Kresling-like patterns unit to conclude the elongation.

Experimental equipment

A digital air pump (Lab vp15-d12, Kamoer Co.,Ltd., China) which can output the air flow rate ranging from 4 L/min to 12 L/min was used to generate the positive pressure and the negative pressure for the SPA. The air pump was driven by a DC brush motor. A 251 mm × 300 mm × 400 mm aluminum framework with a stepping motor (42BYGH34, Pufeide Co.,Ltd., China) was used to realize the horizontal and vertical movement of the SPA. The output force of the SPA was measured by a force gauge (WDF-10 N, WDGAGE Co.,Ltd., China). The measurement range of the force gauge is 0–10 N, the measurement interval is 0.01 N, and the measurement precision is 1%.

Results

The elongation of one-layer kresling-like pattern

As shown in Fig. 4A, we defined the geometric parameters of the skeleton in one Kresling-like pattern: d represents the thickness of a basal plate; d' represents the vertical distance from the bottom surface of the basal plate to the midpoint of the adjacent convex cap; h and l represent the vertical distance and the linear distance between two convex caps in one extensible inserting structure, respectively; Δl represents the length range of an extensible inserting structure; r represents the horizontal distance from the central axis of the Kresling-like unit to the central axis of the vertical cylinder part of a L-shaped part.

The model of extensible inserting structure in the Kresling-like pattern can be simplified into a two-dimensional plane structure for trigonometric function analysis. We further defined m as the third side to construct a triangle together with l and h, as shown in Fig. 4A. When the extensible inserting structure is moving, the values of Δl ($\Delta l < m$), l and h will change. When the Kresling-like pattern unit is fully contracted (i.e., the extensible inserting structure and the basal plate are in parallel), the values of l, h, and m are defined as l_0, h_0, and m_0, respectively, where $h_0 = 0$ and $l_0 = m_0$. When the Kresling-like pattern unit is fully expanded, the values of l, h, and m are defined as l_1, h_1, and m_1, respectively, where $l_1 = l_0 + \Delta l$, $h_1 = h_0 + \Delta h$, and $m_1 = m_0 + \Delta m$. Because the horizontal distance m between two convex caps will not change when the extensible inserting structure is moving, the value of Δm remains 0. According to the Pythagorean Theorem, Δh can be calculated by

$$\Delta h = h = \sqrt{l^2 - m^2} \tag{1}$$

where the higher value of l and the lower value of m result in the higher value of Δh.

Ignoring the thickness of the protruding cylinder on the basal plate, the total height of the Kresling-like pattern unit can be expressed as $H = 2(d + d' + h)$. The height of two typical states, i.e., the unit is fully contracted and is fully expanded, can be expressed as

$$\begin{cases} H_0 = 2(d + d' + h_0) = 2(d + d') \\ H_1 = 2(d + d') + \Delta h \end{cases} \tag{2}$$

So the elongation of one Kresling-like pattern unit can be calculated as:

$$e = \frac{H_1 - H_0}{H_0} \times 100\% = \frac{\Delta h}{2(d + d')} \times 100\% = \frac{\sqrt{l^2 - m^2}}{2(d + d')} \times 100\% \tag{3}$$

We further simplify the Kresling-like unit (Fig. 4B) into a two-dimensional shape in Fig. 4C from top view. Two triangles $\triangle ABC$ and $\triangle DEF$ denote two basal plates in one Kresling-like pattern; the vertexes of two triangles locate at the central axes of the vertical cylinders of the L-shaped parts; three dash-dotted lines represent three extensible inserting structures, e.g., the dash-dotted line GH is one extensible inserting structure which is used to connect two L-shaped parts with the central axes through D and C. In Fig. 4C, values of m and r are same, and we defined $l = l_0 + \Delta l$ and $l_0 = m_0 = r$, so the elongation of one Kresling-like pattern can be further expressed as

$$e = \frac{\sqrt{l^2 - r^2}}{2(d + d')} \times 100\% = \frac{\sqrt{\Delta l^2 + 2r\Delta l}}{2(d + d')} \times 100\% (\Delta l < r) \tag{4}$$

When we set Δl = 8.64 mm, r = 17.96 mm, d = 3.00 mm, and d'=4.50 mm, the elongation's theoretical value (e) of a one-layer Kresling-like pattern is approximately equal to 130.80% according to Eq. (2). We also used SOLIDWORKS software to verify the accuracy of Eq. (2) by building a model with same parameters, and the value of the elongation we concluded was equal to the theoretical value.

The elongation of multi-layer kresling-like pattern

By disassembling or assembling Kresling-like units, we can adjust the number of layers of Kresling-like pattern. When the number of layers is n, the height of the fully contracted unit (H_0) and the fully expanded unit (H_1) is

$$\begin{cases} H_0 = d(n + 1) + 2d'n \\ H_1 = H_0 + n\Delta h \end{cases} \tag{5}$$

The elongation of the multi-layered Kresling-like units can be expressed as

$$e = \frac{H_1 - H_0}{H_0} \times 100\% = \frac{n\Delta h}{d(n + 1) + 2d'n} \times 100\% \tag{6}$$

According to Eq. (4), the relation between Δh and two predefined parameters (r and Δl) can be written as

$$\Delta h = \sqrt{\Delta l^2 + 2r\Delta l} (\Delta l < r) \tag{7}$$

According to Eq. (6) and Eq. (7), the elongation of the multi-layered Kresling-like units can be further expressed as

$$e = \frac{n\sqrt{\Delta l^2 + 2r\Delta l}}{d(n + 1) + 2d'n} \times 100\% (\Delta l < r) \tag{8}$$

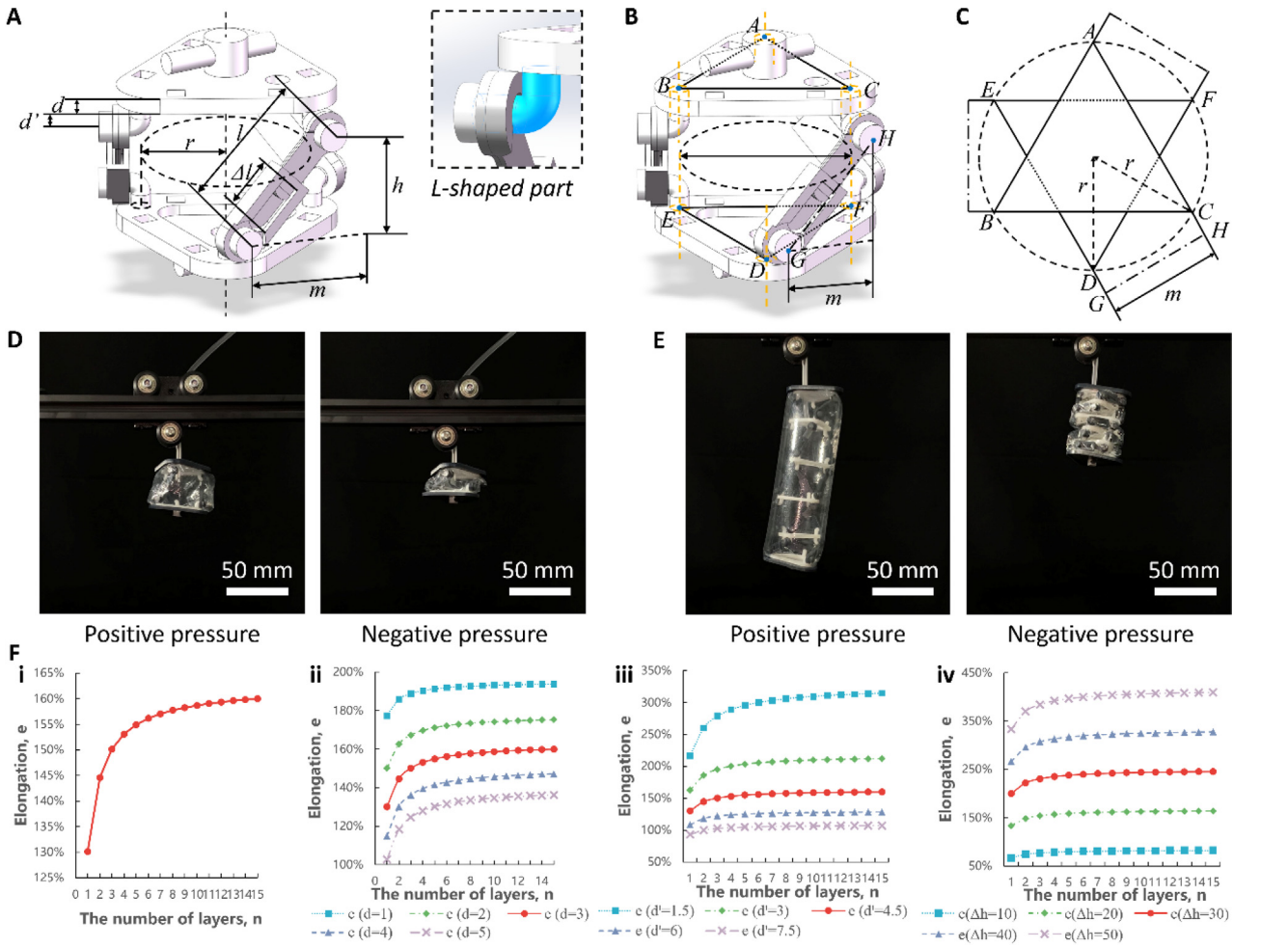

Fig. 4. Geometry of a Kresling-like pattern unit and its elongation. (A) Geometric parameters for the Kresling-like pattern unit and the L-shaped part. (B) A simplified model for the Kresling-like pattern unit. The vertexes of two triangles locate at the central axes of the vertical cylinders of the L-shaped parts. (C) A two-dimensional shape of the Kresling-like pattern unit from top view. Two triangles $\triangle ABC$ and $\triangle DEF$ denote two basal plates in one Kresling-like pattern; three dash-dotted lines represent three extensible inserting structures, e.g., the dash-dotted line *GH* is one extensible inserting structure which is used to connect two L-shaped parts with the central axes through *D* and *C*. (D) The contraction motion of one SPA with one-layer Kresling-like pattern when the internal pressure is from positive to negative. (E) The contraction motion of one SPA with five-layer Kresling-like pattern when the internal pressure is from positive to negative. (F) The relation between the elongation of the SPA and geometric parameters (i: the number of layers of Kresling-like patterns (n); ii: the thickness of a basal plate(d); iii: the vertical distance from the bottom surface of the basal plate to the midpoint of the adjacent convex cap (d'); iv: the vertical extensible distance of one extensible inserting structure (Δh)).

Eq. (8) reveals the relations of the geometric parameters (Δl, r, d, and d') and the elongation of multi-layered Kresling-like patterns. When we set Δl = 8.64 mm, r = 17.96 mm, d = 3.00 mm, and d'=4.50 mm, the elongation's theoretical value (e) of a three-layer (n = 3) Kresling-like pattern and a four-layer (n = 4) Kresling-like pattern is approximately equal to 150.15% and 153.10%, respectively.

We also tested the actual contraction/expansion motions of the SPA with one-layer and multi-layer Kresling-like patterns encapsulated in a soft skin to evaluate the elongations. Fig. 4D and Fig. 4E show the fully contracted/expanded states of one SPA with one-layer Kresling-like pattern and one SPA with multi-layer Kresling-like pattern, respectively.

We further explored the relation between the elongation and the number of layers of Kresling-like patterns (n), and the elongation can be expressed as

$$e = \frac{n\Delta h}{d(n+1)+2d'n} \times 100\% = \frac{1}{\frac{d+2d'}{\Delta h}+\frac{d}{n\Delta h}} \times 100\% \quad (9)$$

where e increases as n increases, and the increasing rate of e shows a tendency to decline (Fig. 4F **(i)**). The elongation increases greatly when the number of layers is lower than five, and increases slowly when the number of layers is higher than five. When the number of layers of Kresling-like patterns is close to positive infinity, its elongation tends to

$$\lim_{n\to\infty} e = \frac{\Delta h}{d+2d'} \quad (10)$$

The maximum elongation of the SPA tends to 162.67%.

Then, we investigated the effect of d, d', and Δh on e. Fig. 4F **(ii - iv)** respectively shows the relation between e and these relevant parameters. And different curves represent different elongations with different values of d ranging from 1 to 5 mm, d' ranging from 1.5 to 7.5 mm, and Δh ranging from 10 to 50 mm, respectively. As shown in Fig. 4F **(ii - iv)**, the elongation increases as d or d' decreases, and increases as Δh increases.

The relation between the output force and negative pressure

Fig. 5A shows experimental devices for investigating the relation between the output force and negative pressure (vacuum). The negative pressure was adjusted by an air pump (Lab vp15-

d12, Kamoer Co.,Ltd., China), the output force of the SPA was measured by a force gauge (WDF-10 N, WDGAGE Co.,Ltd., China), and the motion of the SPA was recorded by a camera. The output force generated by the contraction motion of the SPA was measured by the force gauge under flow rate of 4 L/min. We first applied a constant fluidic output with an air flow rate set at 4 L/min into the SPA with the three-layer Kresling-like pattern to generate relative negative pressure; then, the flow rate was increased 1 L/min per measurement until the flow rate reached to 10 L/min. For each flow rate, we repeated the measurement for 7 times, and the median value of the output force for all 7 measurements was used as the final value. The experimental results are shown in Fig. 5B. The horizontal axis represents the air flow rate, and the vertical axis represents the output force generated by the SPA. A prediction line of the output force is fitted based on the recorded data, and can be expressed as

$$y = 0.5914x + 0.5529 \tag{11}$$

where $\times$ represents the air flow rate ($x \geq 4$ L/min), and y represents the output force F.

The relation between the output force and the number of layers

The peak output forces of five SPAs with different numbers of layers of Kresling-like patterns (one-layer to five-layer) are measured by the force gauge under a flow rate set at 5 L/min. For each number of layers, we repeated the measurement for 7 times, and the median value of the output force for all 7 measurements was used as the final value. The experimental results are shown in Fig. 5C. The horizontal axis represents the number of layers of Kresling-like patterns, and the vertical axis represents the output force generated by the SPA. A natural logarithmic curve is fitted to predict the potential relation between the output force and the number of layers, and can be expressed as

$$y = 1.0587\ln(x) + 2.36 \tag{12}$$

where $\times$ represents the number of layers of the SPA ($x \in N^*$), and y represents the output force F.

The bending performance

With the understanding of the multimodal deformation of Kresling patterns through external forces or constraints, we further exploit the bending performance of the SPA through unequal distribution of external forces [22]. In our study, we used the multi-shape skins shaped by a heat sealer to constrain the contraction/-expansion states of SPAs [6,48]. As shown in Fig. 5D and Movie S2, we used a straight tube-shaped skin and a curved tube-shaped skin to test the flexibility and the bending performance of an SPA with five-layer Kresling-like patterns. The changes of the length of all extensible inserting structures are same when the SPA with the straight tube-shaped skin is fully inflated, so the SPA performs an axial expansion motion. Due to the fixed expansion shape of the curved tube-shaped skin, the changes of the length of all extensible inserting structures are different (i.e., the changes of the length of the extensible inserting structures on the left side (long edge) are greater than those on the right side (short edge)) when the SPA is fully inflated, so the SPA performs a bending motion.

The flexibility and bending performance of the SPA can be applied for soft grippers to grab objects. As shown in Fig. 5E and Movie S3, we fabricated a soft gripper which is composed of two same SPAs with five-layer Kresling-like patterns in the curved tube-shaped skin. The two SPAs can perform the bending motion when they are fully inflated, and the soft gripper can successfully

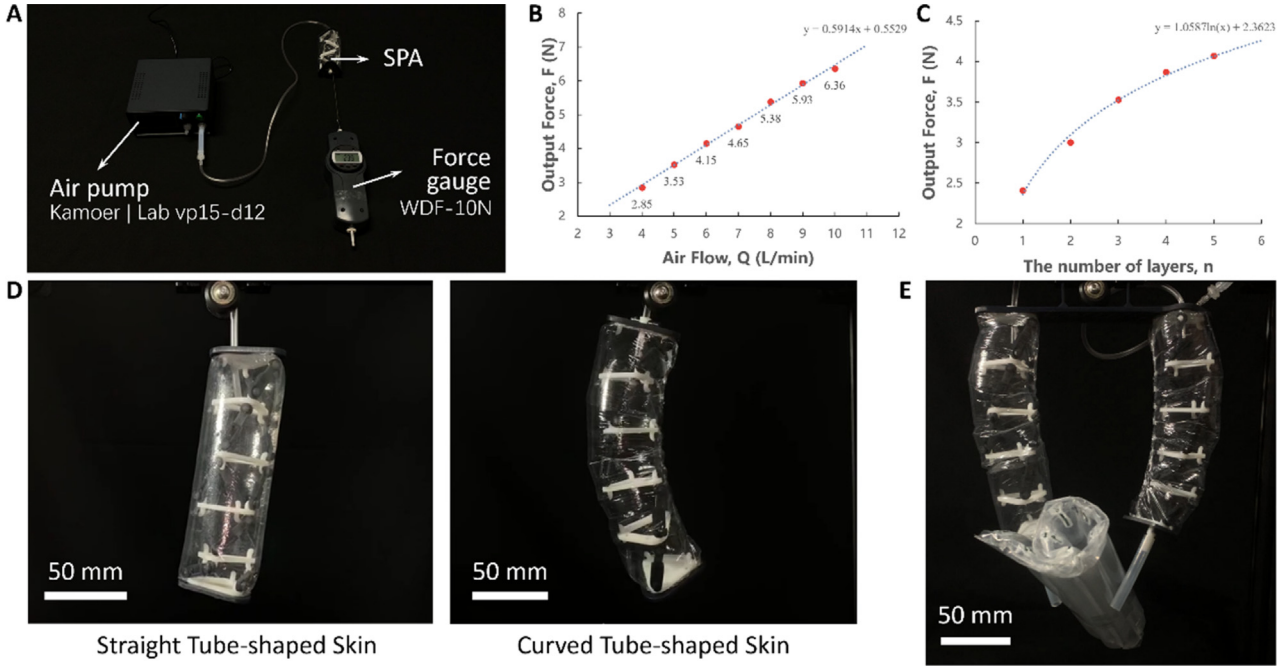

Fig. 5. The output force and the flexibility. (A) Experimental devices for measuring the output force of the SPA. The negative pressure was adjusted by an air pump (Lab vp15-d12, Kamoer Co.,Ltd., China), the output force of the SPA was measured by a force gauge (WDF-10 N, WDGAGE Co.,Ltd., China), and the motion of the SPA was recorded by a camera. (B) The prediction line to predict the potential relation between the output force and the air flow rate. The horizontal axis represents the air flow rate, and the vertical axis represents the output force generated by the SPA. (C) The logarithmic curve to predict the potential relation between the output force and the number of layers. The horizontal axis represents the number of layers of Kresling-like patterns, and the vertical axis represents the output force generated by the SPA. (D) The expansion states of SPAs with the straight tube-shaped skin and the curved tube-shaped skin. (E) A soft gripper which is composed of two same SPAs with five-layer Kresling-like patterns in the curved tube-shaped skin. The two SPAs can perform the bending motion when they are fully inflated, and the soft gripper can successfully grab a small bundle of light plastic.

grab a small bundle of light plastic. This application demonstrated the potential use in mimicking the motions of bionic hands.

Comparison between the proposed SPA and other Kresling-based actuators

A comparison between single units of the SPA proposed here and some existing Kresling actuators in terms of their actuation mechanisms, coupled twist, bendability, modularization, elongation and output force can be found in Table 1 [4,27,49]. According to the comparison, the proposed SPA possesses advantages of bendability (our SPA and the SPA in [49]), modularization (our SPA and the SPAs in [27,49]), and removal of coupled twist motion (only our SPA). Although the elongation of the proposed SPA with one-layer Kresling-like pattern is slight less than some of existing Kresling actuators, it can be simply improved by adding layers of Kresling-like patterns. For example, the elongation of an SPA with three-layer Kresling-like patterns is 153.10%, which is quite close to some existing Kresling-based actuators.

Applications of the SPA with kresling-like patterns

We used the SPAs to develop more applications based on their motion characteristics (axial contraction/expansion motion and bending motion). To transfer force more effectively, we redesigned the sealing cover used in the general SPA for some applications. The new sealing cover (multi-leaf sealing cover) can connect external mechanical components by bolts, as shown in Fig. 6A.

Fig. 6B and Movie S4 show an application of a 3D-printing Scissor Gripper actuated by an SPA with two-layer Kresling-like patterns. The Scissor Gripper consists of two scissor-shaped components. The two components are fixed by a bolt in the middle position of them; the end of two components is connected to the multi-leaf sealing cover by a bolt. The SPA can actuate the Scissor Gripper to move like a scissor by the axial contraction/expansion motion. Fig. 6B and Movie S4 show that the tape is gradually lifted and put down by the Scissor Gripper at the flow rate of 9.6 L/min; Fig. 6C and Movie S4 show that the Scissor Gripper is held by hand to grasp a tape at the flow rate of 12 L/min.

Inspired by the claw in the doll-gripping machines, we developed an application of a 3D-printing three-finger Claw Gripper actuated by an SPA with three-layer Kresling-like patterns, as shown in Fig. 6D and Movie S5. The Claw Gripper consists of three finger-shaped components. The SPA can actuate the three components of the Claw Gripper to open and close simultaneously like a claw by the axial contraction/expansion motion. Fig. 6D and Movie S5 show that a 5.00 g badminton is lifted and moved from the left side to the right side by the Claw Gripper.

In addition, we connected the air tubes to two ends of the SPA by inflation and deflation to realize an autonomous crawling motion of the SPA. Due to the flexibility and bending performance of the SPA, it can perform the crawling motion in multi-shaped pipes [28,50]. This application is expected to be further developed for some special works in narrow environments, such as general maintenance of the city pipeline. Fig. 6E and Movie S6 show that an application of a Pipe Crawler actuated by an SPA with three-layer Kresling-like patterns in the straight tube-shaped skin crawls through a transparent straight pipe. The inner diameter and length of this pipe are 60 mm and 220 mm, respectively. Fig. 6F and Movie S7 show that an application of a Pipe Crawler actuated by an SPA with three-layer Kresling-like patterns in the curved tube-shaped skin crawls through a transparent curved pipe. The radian, inner diameter and length of this pipe are 1.047 rad, 60 mm and 240.65 mm, respectively. If the SPA is crawling from left to right in the pipe, the steps of one crawling cycle of the SPA are as follows: (1) fix the air tube which is connecting to the left end of the SPA, and free the air tube which is connecting to the right end of the SPA; (2) inflate fully through the air tube which is connecting to the left end to generate positive pressure, and the SPA performs the expansion motion and moves forward; (3) fix the air tube which is connecting to the right end of the SPA, and free the air tube which is connecting to the left end of the SPA; (4) deflate fully through the air tube which is connecting to the right end to generate negative pressure, and the SPA performs the contraction motion and moves forward. For each cycle, the SPA can move forward about H_0 (the length of the fully contracted SPA) $\times$ e (the elongation of the SPA), i.e., about 58.56 mm in the straight pipe of Fig. 6E.

Discussion

In our paper, we proposed a soft pneumatic actuator (SPA) based on a Kresling-like pattern with a rigid skeleton. The shape and modularization of the proposed SPA are designed based on the inspiration from salps. The cloning behavior and releasing behavior of salps inspire us to form the SPA with multiple layers of the same skeletons that can be disassembled/assembled repeatedly. And just like salps in one chain are fed by one shared passage, all units of skeletons of one Kresling-like SPA share one air passage and contract/expand together. These units, i.e., Kresling-like patterns, are transformed from the traditional Kresling patterns. We used the extensible inserting structure to replace the creases in traditional Kresling patterns in this SPA, resulting in no twisting motion when the SPA performs the axial contraction/expansion motion and improving the elongation further. Experiments were designed to investigate the relation between geometric parameters and the elongation of the SPA. According to Eq. (4) and Eq. (9), the elongation can be improved by increasing the horizontal distance from the central axis of the Kresling-like unit to the central axis of the vertical cylinder part of a L-shaped part (r), increasing the length range of an extensible inserting structure (Δl), decreasing the thickness of a basal plate (d), and decreasing the vertical distance from the bottom surface of the basal plate to the midpoint of the adjacent convex cap (d'). For the SPAs with same geometric parameters, the elongation can be further improved by increasing the number of layers of Kresling-like patterns (n), but the increasing rate of the elongation shows a tendency to decline as n increases. According to Fig. 4F **(ii)**, for each n, e decreases as d

Table 1
Comparison between units of the proposed SPA and other Kresling-based actuators reviewed.

	SPA with Kresling-like patterns	***Small-scale origami crawler***	***vacuum-powered SPA***	***cube-shaped SPAs***
Actuation	Air flow (5 L/min)	Magnetic(40 mT)	Vacuum (-80 kPa)	Vacuum (-30 kPa)
Coupled twist	0°	32°	~70°	60°
Bendability	Y	N	N	Y
Modularization	Y	N	Y	Y
Elongation	130.80%	~150%	~180%	~160%
Ref	This work	[4]	[27]	[49]

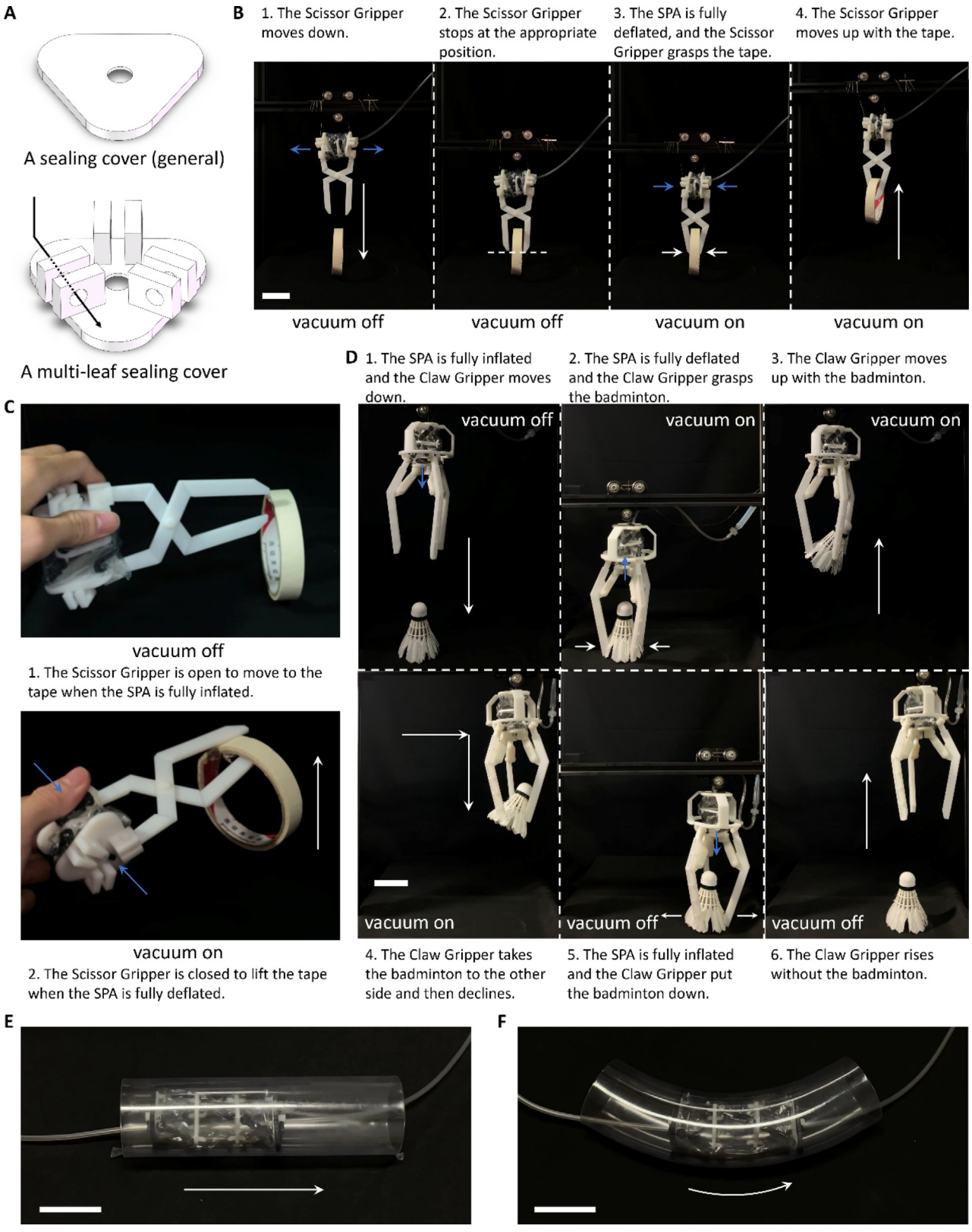

Fig. 6. Applications of the SPA with Kresling-like patterns. (A) The general sealing cover and the multi-leaf sealing cover. The multi-leaf sealing cover can connect external mechanical components by bolts for some applications. (B) An application of a 3D-printing Scissor Gripper actuated by an SPA with two-layer Kresling-like patterns. The Scissor Gripper consists of two scissor-shaped components. The SPA can actuate the Scissor Gripper to move like a scissor by the axial contraction/expansion motion. The tape is gradually lifted and put down by the Scissor Gripper. (C) The Scissor Gripper is held by hand to grasp a tape. (D) An application of a 3D-printing three-finger Claw Gripper actuated by an SPA with three-layer Kresling-like patterns. The Claw Gripper consists of three finger-shaped components. The SPA can actuate the three components of the Claw Gripper to open and close simultaneously like a claw by the axial contraction/expansion motion. A 5.00 g badminton is lifted and moved from the left side to the right side by the Claw Gripper. (E) An application of a Pipe Crawler actuated by an SPA with three-layer Kresling-like patterns in the straight tube-shaped skin crawls through a transparent straight pipe. The inner diameter and length of this pipe are 60 mm and 220 mm, respectively. (F) An application of a Pipe Crawler actuated by an SPA with three-layer Kresling-like patterns in the curved tube-shaped skin crawls through a transparent curved pipe. The radian, inner diameter and length of this pipe are 1.047 rad, 60 mm and 240.65 mm, respectively.

increases, and the decreasing rate of e shows a tendency to decline; for the same Δn, the value of e increases faster when the value of d is higher, e.g., the difference between the elongations of one-layer (n = 1) and three-layer (n = 3) SPAs when d is 5 mm is greater than the difference between the elongations of one-layer (n = 1) and three-layer (n = 3) SPA when d is 1 mm. According to Fig. 4F **(iii)**, for each n, e decreases as d' increases, and the decreasing rate of e shows a tendency to decline; for the same Δn, the value of e increases slower when the value of d' is higher, e.g., the difference between the elongations of one-layer (n = 1) and three-layer (n = 3) SPAs when d' is 7.5 mm is lesser than the difference between the elongations of one-layer (n = 1) and three-layer (n = 3) SPA when d' is 1.5 mm. According to Fig. 4F **(iv)**, for each n, e increases as Δh increases, and the increasing rate of e shows a tendency to rise; for the same Δn, the value of e increases faster when the value of d' is higher, e.g., the difference between the elongations of one-layer (n = 1) and three-layer (n = 3) SPAs when Δh is 50 mm is greater than the difference between the elongations of one-layer (n = 1) and three-layer (n = 3) SPA when Δh is 10 mm.

The experimental results also demonstrate that the air flow generated by the air pump and the number of layers of Kresling-like patterns can affect the output force performance of the SPA. Compared to some existing methods [51,52], our method by changing the air flow and the number of layers is easier to adjust output force. Fig. 5B shows that the output force of the SPA is proportional to the air flow rate, i.e., the output force increases as the air flow rate increases. Fig. 5C shows that the output force of the SPA increases synchronously with the increase of the number of layers (n). The increasing rate of the output force shows a tendency to decline as n increases, so we used a logarithmic curve to describe the potential relation between the output force and the number of layers. In addition, we used a curved tube-shaped skin out of the Kresling-like patterns to realize the bending motion which is hard to perform in the traditional SPA with Kresling patterns. This motion characteristic can be used in some complex application scenarios where both the axial contraction/expansion motion and the bending motion are needed. We also compared the proposed SPA with other existing Kresling-based actuators, some unique advantages of the actuator like bendability, modularization, and removal of the coupled twist were found.

Considering all kinds of potential application scenarios for our SPA to act as an omni-purpose SPA, we designed the SPA taking its adaptability and safety into account. On the one hand, we used PE to fabricate the soft skin of the SPA and use airflow to actuate our SPA in consideration of safety and mimicking salps. On the other hand, we enhanced adaptability through modular design to allow our actuators being applied in various application scenarios.

It should be noted that PE is the sample material for the skin in our study, and the elongation and output force of the SPAs were tested using the skins with this material. Some other materials like PVC can be used to try to improve the motion performance and output force performance in our future works. In addition, we fabricate the skeleton of the SPA with non-recyclable 3D printing resin. If full lifecycle of the SPA is required, the clean manufacture and recyclable materials as reported in [38] will be considered in our future design.

Conclusion

For the SPAs we fabricated in this study, the elongation can reach to 150% when the number of layers is three. By simply adding layers of Kresling-like patterns, the elongation can increase to above 162%. This value of elongation is very close to some existing traditional Kresling-based actuators, and it can be further improved by adjusting geometric parameters of the SPA. Based on the above experimental results, we developed three potential applications (Scissor Gripper, Claw Gripper and Pipe Crawler) to demonstrate the feasibility of the SPAs in practical use. The Scissor Gripper and the Claw Gripper can be used to grasp and lift objects like a bionic hand [53], and the Pipe Crawler can be used to work in the narrow pipeline environments. Users can add/reduce the layers of Kresling-like patterns for the SPAs and add/reduce the external 3D-printing components by themselves according to the practical needs, which meets users' requirements for modularization and customization. The mixed characteristic of rigidity and flexibility enables the SPA to construct various actuator systems for bionic machines, bionic limbs, bio-inspired robotics and medical devices. The motion characteristic and the modularization characteristic help the SPA adapt the changeable working environments, and extend to more application scenarios in the future.

Compliance with Ethics Requirements

This article does not contain any studies with human or animal subjects

CRediT authorship contribution statement

Zhichuan Tang: Conceptualization, Methodology, Supervision. **Keshuai Yang:** Data curation, Writing – original draft. **Hang Wang:** Visualization. **Zhixuan Cui:** Software. **Xiaoneng Jin:** Investigation. **Yuxin Peng:** Validation. **Pengcheng Liu:** Writing – review & editing.

Declaration of Competing Interest

The authors declare that they have no known competing financial interests or personal relationships that could have appeared to influence the work reported in this paper.

Acknowledgment

This work was supported by the National Natural Science Foundation of China (61702454, 52105563), and the Key Research and Development Program of Zhejiang Province (2022C03148).

Appendix A. Supplementary material

Supplementary data to this article can be found online at https://doi.org/10.1016/j.jare.2023.10.004.

References

[1] Wallin TJ, Pikul J, Shepherd RF. 3D printing of soft robotic systems. Nat Rev Mater 2018;3:84–100. doi: https://doi.org/10.1038/s41578-018-0002-2.
[2] Poccard-Saudart J, Xu S, Teeple CB, Hyun N-S, Becker KP, Wood RJ. Controlling Soft Fluidic Actuators Using Soft DEA-Based Valves. IEEE Robot Autom Lett 2022;7(4):8837–44.
[3] Onal CD, Rus D. Autonomous undulatory serpentine locomotion utilizing body dynamics of a fluidic soft robot. Bioinspir Biomim 2013;8:. doi: https://doi.org/10.1088/1748-3182/8/2/026003026003.
[4] Ze Q, Wu S, Nishikawa J, Dai J, Sun Y, Leanza S, et al. Soft robotic origami crawler. Sci Adv 2022;8(13).
[5] Runciman M, Darzi A, Mylonas GP. Soft Robotics in Minimally Invasive Surgery. Soft Robot 2019;6:423–43. doi: https://doi.org/10.1089/soro.2018.0136.
[6] Chauhan M, Chandler JH, Jha A, Subramaniam V, Obstein KL, Valdastri P. An Origami-Based Soft Robotic Actuator for Upper Gastrointestinal Endoscopic Applications. Front Robot AI 2021;8.
[7] Wang H, Abu-Dakka FJ, Nguyen Le T, Kyrki V, Xu H. A Novel Soft Robotic Hand Design With Human-Inspired Soft Palm: Achieving a Great Diversity of Grasps. IEEE Rob Autom Mag 2021;28:37–49. doi: https://doi.org/10.1109/MRA.2021.3065870.
[8] Zhao H, O'Brien K, Li S, Shepherd RF. Optoelectronically innervated soft prosthetic hand via stretchable optical waveguides. Sci Rob 2016;1(1).

[9] Navarro SE, Nagels S, Alagi H, Faller L-M, Goury O, Morales-Bieze T, et al. A Model-Based Sensor Fusion Approach for Force and Shape Estimation in Soft Robotics. IEEE Robot Autom Lett 2020;5(4):5621–8.
[10] Sareen H, Umapathi U, Shin P, Kakehi Y, Ou J, Ishii H, et al. Printflatables: Printing Human-Scale, Functional and Dynamic Inflatable Objects. Proc. 2017 CHI Conf. Hum. Factors Comput. Syst., Denver Colorado USA: ACM; 2017, p. 3669–80. 10.1145/3025453.3025898.
[11] Park Y-L, Chen B-R, Pérez-Arancibia NO, Young D, Stirling L, Wood RJ, et al. Design and control of a bio-inspired soft wearable robotic device for ankle–foot rehabilitation. Bioinspiration Ampmathsemicolon Biomim 2014;9(1). doi: https://doi.org/10.1088/1748-3182/9/1/016007.
[12] Cianchetti M, Laschi C, Menciassi A, Dario P. Biomedical applications of soft robotics. Nat Rev Mater 2018;3:143–53. doi: https://doi.org/10.1038/s41578-018-0022-y.
[13] Polygerinos P, Wang Z, Galloway KC, Wood RJ, Walsh CJ. Soft robotic glove for combined assistance and at-home rehabilitation. Rob Auton Syst 2015;73:135–43. doi: https://doi.org/10.1016/j.robot.2014.08.014.
[14] Qiu Y, Zhang E, Plamthottam R, Pei Q. Dielectric Elastomer Artificial Muscle: Materials Innovations and Device Explorations. Acc Chem Res 2019;52:316–25. doi: https://doi.org/10.1021/acs.accounts.8b00516.
[15] Narumi K, Sato H, Nakahara K, Seong Ya, Morinaga K, Kakehi Y, et al. Liquid Pouch Motors: Printable Planar Actuators Driven by Liquid-to-Gas Phase Change for Shape-Changing Interfaces. IEEE Robot Autom Lett 2020;5(3):3915–22.
[16] Ze Q, Kuang X, Wu S, Wong J, Montgomery SM, Zhang R, et al. Magnetic Shape Memory Polymers with Integrated Multifunctional Shape Manipulation. Adv Mater 2020;32(4). doi: https://doi.org/10.1002/adma.201906657.
[17] Hines L, Petersen K, Lum GZ, Sitti M. Soft Actuators for Small-Scale Robotics. Adv Mater 2017;29:1603483. doi: https://doi.org/10.1002/adma.201603483.
[18] Ma Z, Sameoto D. A Review of Electrically Driven Soft Actuators for Soft Robotics. Micromachines 2022;13:1881. doi: https://doi.org/10.3390/mi13111881.
[19] Lin Y, Yang G, Liang Y, Zhang C, Wang W, Qian D, et al. Controllable Stiffness Origami "Skeletons" for Lightweight and Multifunctional Artificial Muscles. Adv Funct Mater 2020;30(31). doi: https://doi.org/10.1002/adfm.202000349.
[20] Polygerinos P, Correll N, Morin SA, Mosadegh B, Onal CD, Petersen K, et al. Soft Robotics: Review of Fluid-Driven Intrinsically Soft Devices; Manufacturing, Sensing, Control, and Applications in Human-Robot Interaction. Adv Eng Mater 2017;19(12). doi: https://doi.org/10.1002/adem.201700016.
[21] Rothemund P, Ainla A, Belding L, Preston DJ, Kurihara S, Suo Z, et al. A soft, bistable valve for autonomous control of soft actuators. Sci Rob 2018;3(16).
[22] Wu S, Ze Q, Dai J, Udipi N, Paulino GH, Zhao R. Stretchable origami robotic arm with omnidirectional bending and twisting. Proc Natl Acad Sci 2021;118:e2110023118. 10.1073/pnas.2110023118.
[23] Kobayashi H, Kresling B, Vincent JFV. The geometry of unfolding tree leaves. Proc R Soc Lond B Biol Sci 1998;265:147–54. doi: https://doi.org/10.1098/rspb.1998.0276.
[24] Kaufmann J, Bhovad P, Li S. Harnessing the Multistability of Kresling Origami for Reconfigurable Articulation in Soft Robotic Arms. Soft Robot 2022;9:212–23. doi: https://doi.org/10.1089/soro.2020.0075.
[25] Lu L, Dang X, Feng F, Lv P, Duan H. Conical Kresling origami and its applications to curvature and energy programming. Proc R Soc Math Phys Eng Sci 2022;478:20210712. doi: https://doi.org/10.1098/rspa.2021.0712.
[26] Zhang Z, Chen G, Wu H, Kong L, Wang H. A Pneumatic/Cable-Driven Hybrid Linear Actuator With Combined Structure of Origami Chambers and Deployable Mechanism. IEEE Robot Autom Lett 2020;5:3564–71. doi: https://doi.org/10.1109/LRA.2020.2976324.
[27] Jin T, Li L, Wang T, Wang G, Cai J, Tian Y, et al. Origami-Inspired Soft Actuators for Stimulus Perception and Crawling Robot Applications. IEEE Trans Rob 2022;38(2):748–64.
[28] Jiang C, Pei Z. An in-pipe worm robot with pneumatic actuators based on origami paper-fabric composites. Text Res J 2021;91:2724–37. doi: https://doi.org/10.1177/00405175211016561.
[29] Terryn S, Brancart J, Lefeber D, Van Assche G, Vanderborght B. Self-healing soft pneumatic robots. Sci Rob 2017;2(9).
[30] Bhovad P, Kaufmann J, Li S. Peristaltic locomotion without digital controllers: Exploiting multi-stability in origami to coordinate robotic motion. Extreme Mech Lett 2019;32:. doi: https://doi.org/10.1016/j.eml.2019.100552100552.
[31] Pagano A, Yan T, Chien B, Wissa A, Tawfick S. A crawling robot driven by multi-stable origami. Smart Mater Struct 2017;26(9). doi: https://doi.org/10.1088/1361-665X/aa721e.
[32] Yap HK, Ng HY, Yeow C-H. High-Force Soft Printable Pneumatics for Soft Robotic Applications. Soft Robot 2016;3:144–58. doi: https://doi.org/10.1089/soro.2016.0030.
[33] Tawk C, Panhuis M in het, Spinks GM, Alici G. 3D Printed Soft Pneumatic Bending Sensing Chambers for Bilateral and Remote Control of Soft Robotic Systems. 2020 IEEEASME Int. Conf. Adv. Intell. Mechatron. AIM, Boston, MA, USA: IEEE; 2020, p. 922–7. 10.1109/AIM43001.2020.9158959.
[34] Lee K, Jung P-G, Cha Y. Origami Pump Based on Planetary Gear System for Pneumatic Pressure. IEEEASME Trans Mechatron 2022:1–10. doi: https://doi.org/10.1109/TMECH.2022.3223699.
[35] Philamore H, Ieropoulos I, Stinchcombe A, Rossiter J. Toward Energetically Autonomous Foraging Soft Robots. Soft Robot 2016;3:186–97. doi: https://doi.org/10.1089/soro.2016.0020.
[36] Li G, Chen X, Zhou F, Liang Y, Xiao Y, Cao X, et al. Self-powered soft robot in the Mariana Trench. Nature 2021;591(7848):66–71.
[37] Cianchetti M, Ranzani T, Gerboni G, Nanayakkara T, Althoefer K, Dasgupta P, et al. Soft Robotics Technologies to Address Shortcomings in Today's Minimally Invasive Surgery: The STIFF-FLOP Approach. Soft Robot 2014;1(2):122–31.
[38] Rayner P, Morita L, Sun X, Sameoto D. R3VAMPs - Fully Recyclable, Reconfigurable, and Recoverable Vacuum Actuated Muscle-inspired Pneumatic structures. 2022 IEEE 5th Int. Conf. Soft Robot. RoboSoft, 2022, p. 577–82. 10.1109/RoboSoft54090.2022.9762163.
[39] Kim W, Byun J, Kim J-K, Choi W-Y, Jakobsen K, Jakobsen J, et al. Bioinspired dual-morphing stretchable origami. Bioinspired dual-morphing stretchable origami Sci Robot 2019;4(36). doi: https://doi.org/10.1126/scirobotics.aay3493.
[40] Hirose E, Kimura S, Itoh T, Nishikawa J. Tunic Morphology and Cellulosic Components of Pyrosomas, Doliolids, and Salps (Thaliacea, Urochordata). Biol Bull 1999;196:113–20. doi: https://doi.org/10.2307/1543173.
[41] Sutherland KR, Weihs D. Hydrodynamic advantages of swimming by salp chains. J R Soc Interface 2017;14:20170298. doi: https://doi.org/10.1098/rsif.2017.0298.
[42] Stone JP, Steinberg DK. Long-term time-series study of salp population dynamics in the Sargasso Sea. Mar Ecol Prog Ser 2014;510:111–27. doi: https://doi.org/10.3354/meps10985.
[43] Drotman D, Ishida M, Jadhav S, Tolley MT. Application-Driven Design of Soft, 3-D Printed, Pneumatic Actuators With Bellows. IEEEASME Trans Mechatron 2019;24:78–87. doi: https://doi.org/10.1109/TMECH.2018.2879299.
[44] Kidambi N, Wang KW. Dynamics of Kresling origami deployment. Phys Rev E 2020;101:. doi: https://doi.org/10.1103/PhysRevE.101.063003063003.
[45] Wang X, Qu H, Guo S. Tristable property and the high stiffness analysis of Kresling pattern origami. Int J Mech Sci 2023;256:. doi: https://doi.org/10.1016/j.ijmecsci.2023.108515108515.
[46] Li Z, Kidambi N, Wang L, Wang K-W. Uncovering rotational multifunctionalities of coupled Kresling modular structures. Extreme Mech Lett 2020;39:. doi: https://doi.org/10.1016/j.eml.2020.100795100795.
[47] Novelino LS, Ze Q, Wu S, Paulino GH, Zhao R. Untethered control of functional origami microrobots with distributed actuation. Proc Natl Acad Sci 2020;117:24096–101. doi: https://doi.org/10.1073/pnas.2013292117.
[48] Li S, Vogt DM, Rus D, Wood RJ. Fluid-driven origami-inspired artificial muscles. Proc Natl Acad Sci 2017;114:13132–7. doi: https://doi.org/10.1073/pnas.1713450114.
[49] Jin T, Wang T, Xiong Q, Tian Y, Li L, Zhang Q, et al. Modular Soft Robot with Origami Skin for Versatile Applications. Soft Robot 2023;10(4):785–96.
[50] Chen S, Cao Y, Sarparast M, Yuan H, Dong L, Tan X, et al. Soft Crawling Robots: Design, Actuation, and Locomotion. Adv Mater Technol 2020;5:1900837. doi: https://doi.org/10.1002/admt.201900837.
[51] Su H, Hou Xu, Zhang X, Qi W, Cai S, Xiong X, et al. Pneumatic Soft Robots: Challenges and Benefits. Actuators 2022;11(3):92.
[52] Avery J, Runciman M, Darzi A, Mylonas GP. Shape Sensing of Variable Stiffness Soft Robots using Electrical Impedance Tomography. 2019 Int. Conf. Robot. Autom. ICRA, Montreal, QC, Canada: IEEE; 2019, p. 9066–72. 10.1109/ICRA.2019.8793862.
[53] Kim Y, Cha Y. Soft Pneumatic Gripper With a Tendon-Driven Soft Origami Pump. Front Bioeng Biotechnol 2020;8.